Landslides
DOI 10.1007/s10346-017-0936-2
Received: 12 June 2017
Accepted: 17 December 2017
© Springer-Verlag GmbH Germany, part of Springer Nature 2017

Jing-Sen Cai · Tian-Chyi Jim Yeh · E-Chuan Yan · Rui-Xuan Tang · Jet-Chau Wen · Shao-Yang Huang

An adaptive sampling approach to reduce uncertainty in slope stability analysis

Abstract An adaptive sampling approach is proposed, which can sample spatially varying shear strength parameters efficiently to reduce uncertainty in the slope stability analysis. This approach employs a limit equilibrium model and stochastic conditional methodology to determine the likely sampling locations. Karhunen-Loève expansion is used to conduct the conditional Monte Carlo simulation. A first-order analysis is also proposed to ease the computational burden associated with Monte Carlo simulation. These approaches are then tested using borehole data from a field site. Results indicate that the proposed adaptive sampling approach is an effective and efficient sampling scheme for reducing uncertainty in slope stability analysis.

Keywords Conditional analysis · Sampling approach · Slope stability · Reliability · Shear strength · Spatial variability

Introduction

Physical or mechanical properties (e.g., soil permeability, soil cohesion, or soil friction angle) of geologic formation vary in space at a multiplicity of scales (i.e., variations in the properties between different strata and variations within individual stratum). Unconditional stochastic description of these properties of a geologic medium quantifies their heterogeneity or spatial variability, in a statistical sense without resorting to their detailed spatial distributions. Specifically, it describes the heterogeneity in terms of a probability distribution, characterized by a constant mean (the most likely value of the property), a variance (the average deviation of the mean property from the actual property at different locations), and a correlation structure (i.e., the averaged thickness, width, and length of the soils with similar properties). This stochastic approach has been widely accepted and is proven to be useful in slope stability analysis (e.g., Srivastava et al. 2010; Griffiths et al. 2011; Cho 2014; Jiang et al. 2015; Cai et al. 2017b, c). However, stability analysis based on the unconditional stochastics tends to overestimate uncertainty in the analysis since the unconditional stochastics ignores the knowledge of the properties measured at specific locations at a field site. These measurements at these locations reduce our uncertainty about the variability of the properties at the field site and, in turn, can increase the accuracy of the stability analysis.

In order to circumvent the shortcoming of the unconditional approach, the conditional stochastic approach has been developed over the past few decades. It provides a statistic description of the heterogeneity at locations where no point observation is available but it preserves the sampled or measured properties at sample locations (e.g., Harter and Yeh 1996; Li et al. 2014, 2016b; Cai et al. 2017a). This conditional stochastic analysis allows characterization of a property field at a high resolution if sufficient measurements are available, and facilitates estimations of uncertainty associated with the characterization (Yeh et al. 2015a, b).

Generally, the available observations include direct measurements of properties (e.g., soil cohesion or soil friction angle) or their surrogate measurements (e.g., fluid pressures or stresses—responses of the medium to some excitations, Wang et al. 2016; Li et al. 2016b). In this study, only the effect of direct measurements of the effective cohesion and the effective soil friction angle of the soil is investigated.

Although conditional stochastic approaches have been used in many fields (e.g., Harter and Yeh 1996; Van den Eijnden and Hicks 2011; Lloret-Cabot et al. 2014), few attempts have applied them to evaluations of slope stability and reliability. More importantly, few studies have addressed the salient question: how to collect samples of soil strength in a cost-effective manner to reduce the uncertainty in the slope stability analysis.

Recently, Cai et al. (2016) demonstrated that uncertainty in slope stability analysis is not equally influenced by heterogeneity everywhere within the slope. Likewise, Zhang et al. (2011) and Li et al. (2013) found that the contributions to the slope failure probability are dominated by a limited number of representative slip surfaces. These findings compel us to develop a cost-effective sampling approach to reduce the uncertainty in the analysis. That is, one determines the critical sampling locations and then samples at these locations to adequately characterize the effects of heterogeneity, rather than measures the soil properties everywhere within the slope.

The objective of this study is to develop an adaptive sampling approach to conduct a conditional stochastic analysis of slope stability to reduce uncertainty and to enhance the reliability of the analysis. In order to achieve this objective, we develop a method, based on kriging and Karhunen-Loève (K-L) expansion, for generating random soil strength fields, conditioned on our prior information about the spatial variability and in situ measurements. Afterward, a stochastic limit equilibrium method (LEM, a physical model for assessing slope stability, see "Modeling of FS_i, FS, and Pf" section) is introduced to conduct conditional Monte Carlo simulation (MCS) for identifying possible slip surfaces, which dictate the sampling locations. Further, a first-order analysis approach is presented to ease the computational burden associated with MCS. At last, the proposed sampling approach and associated stochastic analysis tools are applied to a field site.

Adaptive sampling strategy

Slope stability and reliability analysis is an analysis aim to quantify the uncertainty of our decision based on incomplete information about slope stability. While many factors can influence the slope stability (e.g., unknown temporal and spatial distributions of stresses, pore-water pressures, and strengths of a slope), the spatial variability of the shear strength parameters of a slope is the focus in this paper.

Published online: 29 December 2017

Rationale and procedure of the adaptive sampling approach

The rationale and procedure of this adaptive sampling approach are illustrated in Fig. 1. If a slope has n number of potential slip surfaces, and the strength property of each surface is unknown at a given field site, we first conceptualize the spatial distribution of the soil strength property in a slope as a random field. That is to say, with a given spatial statistics (estimated from some available measurements of the properties from the field site or similar geologic settings), there are an infinite number of possible realizations of the spatial distribution of the property and in turn, an infinite number of factors of safety FS_is at the ith potential slip surfaces. Note that the FS_i is evaluated based on the limited equilibrium physical model, LEM (Eq. (16); note $i=1, \cdots, n$), and the given strength properties. This leads to many possible critical slip surfaces within the n potential slip surfaces. In order to narrow down the possible locations of the critical slip surface, the proposed approach calculates the lower bound (LB_i) at the ith slip surface based on all possible FS_is at the slip surface. It then finds the minimum value of the lower bounds (LB_is) of the entire n slip surfaces. This process is illustrated as step 1 in Fig. 1.

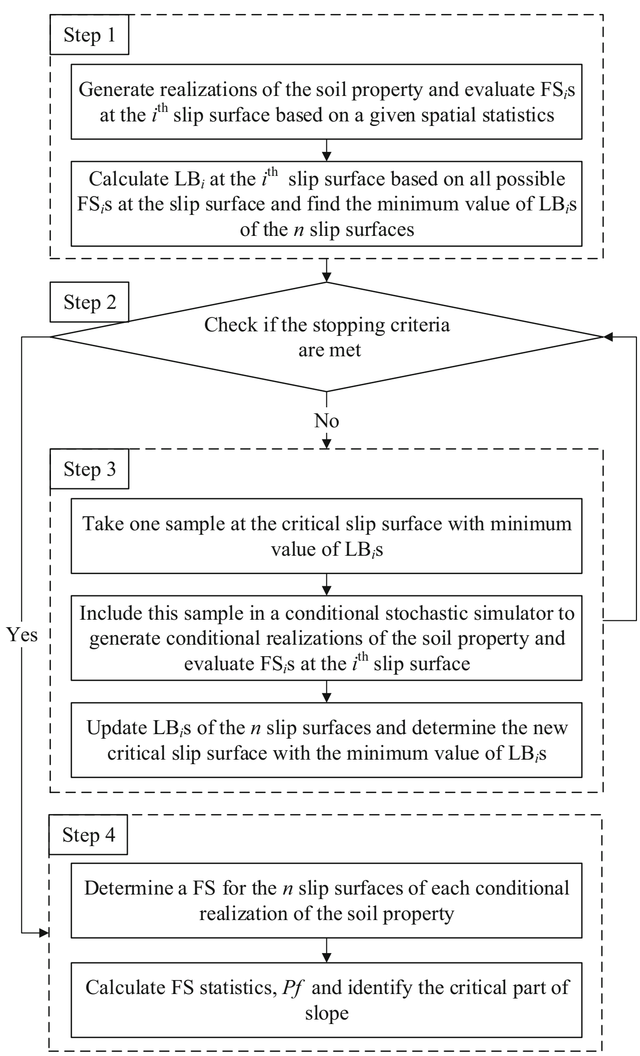

Fig. 1 Flow chart of the adaptive sampling approach

In step 2, we check if any samples should be taken next. Specifically, we check if the first of the three stopping criteria (see "Criteria for stopping the sampling process" section) (i.e., if the probability of failure of the slope equals 1) is met. If it is true, we do not have to take any sample and move to step 4. If the first criterion is not met, we then check the criterion 2 (i.e., if the probability of failure of the slope is sufficiently small). If this criterion is met, we move to step 4. If not, we then check the criterion 3 (i.e., if the budget for sampling runs out). If this criterion is met, we move to step 4. Otherwise, we move to step 3.

In step 3, we take a soil sample to determine soil strength parameter value at the location where the minimum value is. This sample value at this location is then included in a conditional stochastic simulator (see "Conditional stochastic methodology" section) to generate conditional realizations of the parameter field. These realizations honor the same sample value at the sample location, and they are used to update the LB_is at the n potential slip surfaces. Based on this updated LB_is, a new likely critical slip surface (i.e., the minimum value of the LB_is of the n slip surfaces) is determined. Then we move back to step 2. This process cycles between step 2 and step 3 until some stopping criteria are met.

Once the cycling between step 2 and step 3 stops, the approach has already generated conditional realizations of the parameter fields that honor the sample values at all the sample locations. We then determine a FS for the entire n potential slip surfaces (Eq. (17)) of each conditional realization as step 4. Consequently, we have a large number of FS values for the entire slope. From these FS values, we calculate their mean (μ_{FS}) and standard deviation (σ_{FS}) and determine the probability of failure (Pf). Thus, the most likely FS value for the slope and its reliability is addressed.

It is a fact that as the number of samples increases, the standard deviation of FS decreases, and the mean of FS approaches the correct (true) FS. However, the proposed sampling approach based on the minimum LB_is resulting from conditional stochastic analysis identifies the likely critical part of a slope for taking measurements and narrows the possible distribution of heterogeneity. As such, this approach reduces uncertainty in our slope stability analysis with a limited number of samples.

We first consider to use the minimal reliability index (e.g., Christian et al. 1994; Li et al. 2014) to determine the likely critical slip surface and further the sample location. The reliability index is defined as $\beta_i = \left(\mu_{FS_i}-1\right) / \sigma_{FS_i}$, where μ_{FS_i} and σ_{FS_i} are the mean and standard deviation of FS_is at the ith potential slip surfaces, respectively. Note that these means and standard deviations are different from the mean (μ_{FS}) and standard deviation (σ_{FS}) of the possible FSs discussed in the previous paragraph. This reliability index is useful, but when the sample is taken at the ith potential slip surface (measurement errors are considered as negligible), σ_{FS_i} would become 0 (i.e., no uncertainty). This zero uncertainty thus yields an infinite value for β_i. In order to avoid this problem, we use $\mu_{FS_i}-\alpha\sigma_{FS_i}$ (where α is a prescribed constant) as the LB_i of all the realizations of FS_i to determine the next sample location.

Note that $\mu_{FS_i}-3\sigma_{FS_i}$ (when α is set to be 3) would lead to 99.865% of all the realizations of FS_i being higher than $\mu_{FS_i}-3\sigma_{FS_i}$ if the probability distribution of FS_i is normal. This is also valid for log-normal distributed FS_i because conditional log-normal and conditional normal distributions become quite similar as more samples are used to condition, and uncertainty of FS_i becomes small (Griffiths et al. 2011). Therefore, $\mu_{FS_i}-3\sigma_{FS_i}$ is a reasonable approximation of the LB_i. Since μ_{FS_i} and σ_{FS_i} are conditional mean and conditional standard deviation, which changes with the number of samples, the LB_i changes accordingly. Now, we emphasize that the critical slip surface with the minimum of $\mu_{FS_i}-\alpha\sigma_{FS_i}$ values may not be the same as that with the minimum of β_i. Nonetheless, the locations of samples selected according to either minimum $\mu_{FS_i}-\alpha\sigma_{FS_i}$ or minimum β_i criterion will coincide after several critical slip surfaces are identified.

Criteria for stopping the sampling process

Generally, the adaptive sampling process stops (1) if the mean of FS_is (μ_{FS_i}) at the potential slip surface where a sample has been taken is smaller than 1, which implies that the slope is evaluated as unstable using the sample value, the probability of failure Pf equals 1 and additional samples have no effect on Pf. (2) If the minimum value of LB_is ($\mu_{FS_i}-3\sigma_{FS_i}$) is larger than or equal to 1 (i.e., the reliability index $\beta_i = \left(\mu_{FS_i}-1\right)/\sigma_{FS_i} \geq 3$), which implies that Pf is small enough (smaller than 1–99.865% = 0.135% = 0.00135), μ_{FS} is larger than (or equal to) 1, and the uncertainty associated with μ_{FS} is small enough compared with μ_{FS}. Or (3) if the upper limit of the number of samples is reached. This number of samples depends on the goal and budget of the project.

Conditional stochastic methodology

Generating conditioned random soil strength parameter field

The random field theory (Vanmarcke 1977a, b; El-Ramly et al. 2002; Griffiths and Fenton 2004; Cho 2007; Yeh et al. 2015a) is applied in this study to model the spatial variability of soil properties. Each soil property is treated as a random field, $\mathbf{X}$, which is a collection of random variables $(X_1, X_2, \ldots, X_n)^T$ at different locations $\mathbf{z} = (z_1, z_2, \ldots, z_n)^T$ within a bounded domain Ω, described by a joint probability density function with a mean $\mu_{\mathbf{X}}$ and a spatial covariance matrix $\mathbf{R_{XX}}$. In order to obtain a preliminary evaluation of the $\mu_{\mathbf{X}}$ and the standard deviation $\sigma_{\mathbf{X}}$ for a domain, Ω, one may collect some samples at a given field site or one can calculate using available data from a similar geologic setting. In this study, we assume the random field is log-normally distributed (e.g., Parkin et al. 1988; Parkin and Robinson 1992; Phoon and Kulhawy 1999; Brejda et al. 2000; Fenton and Griffiths 2008; Griffiths et al. 2011; Li et al. 2014; Jiang et al. 2015).

Random field $\mathbf{X}$ with log-normal distribution can be normalized and represented in the form of the standard random field, $\mathbf{Y}$, which has zero mean and unit variance. The transformation from $\mathbf{X}$ to $\mathbf{Y}$ is done as follows:

$$\mathbf{X} = \exp(\sigma_{\ln\mathbf{X}}\mathbf{Y} + \mu_{\ln\mathbf{X}}) \tag{1}$$

where $\mu_{\ln\mathbf{X}} = \ln\mu_{\mathbf{X}} - \frac{1}{2}\sigma^2_{\ln\mathbf{X}}$ and $\sigma_{\ln\mathbf{X}} = \sqrt{\ln\left(1 + \left(\sigma_{\mathbf{X}}/\mu_{\mathbf{X}}\right)^2\right)}$ are the mean and standard deviation of the logarithm of $\mathbf{X}$, respectively. Here we say the random field $\mathbf{X}$ is in the physical space, $\boldsymbol{x}$, which is distinguished from the transformed standard normal space $\boldsymbol{y}$.

Correlation scale, λ, is used to represent the distance within which the soil properties are significantly correlated. Physically, the correlation scale describes the average dimensions (e.g., length, thickness) of heterogeneity (e.g., layers, or stratifications) within Ω (see Figures 4.12, 4.13, and 4.14 in Yeh et al. 2015a). It shall be noted that λ is considered as the attribute of Ω and is invariant in terms of transformation between space $\boldsymbol{x}$ and space $\boldsymbol{y}$. Based on λ, an autocorrelation matrix $\mathbf{C_{YY}}$, a statistical measure of the spatial structure (or spatial pattern) of heterogeneity, can be expressed in space $\boldsymbol{y}$ as follows:

$$\mathbf{C_{YY}} = \begin{bmatrix} 1 & \rho_{\Delta_{12}} & \cdots & \rho_{\Delta_{1n}} \\ \rho_{\Delta_{21}} & 1 & \cdots & \rho_{\Delta_{2n}} \\ \vdots & \vdots & \ddots & \vdots \\ \rho_{\Delta_{n1}} & \rho_{\Delta_{n2}} & \cdots & 1 \end{bmatrix} \tag{2}$$

where $\rho_{\Delta_{ij}}$ is the autocorrelation between location z_i and z_j. In this study, a common single exponential autocorrelation function is adopted as follows:

$$\rho_{\Delta_{ij}} = \rho\left(\Delta_{ij}\right) = \exp\left[-\Delta_{ij}/\lambda\right] \tag{3}$$

where $\Delta_{ij} = |z_i - z_j|$ is the absolute distances between location z_i and z_j.

Assume m samples at m sample locations are available in physical space $\boldsymbol{x}$, and they are denoted as $\mathbf{X}_s$. Similarly, $\mathbf{X}_s$ are also transformed into space $\boldsymbol{y}$ using Eq. (1) and denoted as $\mathbf{Y}_s$. The next step is to derive the conditional mean properties and their associated conditional (or residual) covariance. The former represents the most likely properties at locations where no measurements are available, with given measurements at sampling locations, and the latter denotes the likely deviation of the conditional mean from the true properties. Simple kriging is used to accomplish this task. That is, an estimate of $n \times 1$ conditional mean vector $\boldsymbol{\mu}_{\mathbf{Y}|\mathbf{Y}_s}$ and $n \times n$ conditional autocorrelation matrix $\mathbf{C}_{\mathbf{YY}|\mathbf{Y}_s}$, given observed $\mathbf{Y}_s$ is:

$$\boldsymbol{\mu}_{\mathbf{Y}|\mathbf{Y}_s} = \boldsymbol{\omega}^T\mathbf{Y}_s \tag{4}$$

$$\mathbf{C}_{\mathbf{YY}|\mathbf{Y}_s} = \mathbf{C_{YY}} - \left(\boldsymbol{\beta}^T\boldsymbol{\beta}\right) \tag{5}$$

where $\boldsymbol{\omega}$ and $\boldsymbol{\beta}$ are the matrices of kriging weights with the dimension of $m \times n$, which are obtained by solving kriging system equations as follows:

$$\mathbf{C}_{\mathbf{Y}_s\mathbf{Y}_s}\boldsymbol{\omega} = \mathbf{C}_{\mathbf{Y}_s\mathbf{Y}} \tag{6}$$

$$\boldsymbol{\Gamma}_{\mathbf{C}_{\mathbf{Y}_s\mathbf{Y}_s}}\boldsymbol{\beta} = \mathbf{C}_{\mathbf{Y}_s\mathbf{Y}} \tag{7}$$

$$\mathbf{C}_{\mathbf{Y}_s\mathbf{Y}_s} = \boldsymbol{\Gamma}_{\mathbf{C}_{\mathbf{Y}_s\mathbf{Y}_s}}\boldsymbol{\Gamma}^T_{\mathbf{C}_{\mathbf{Y}_s\mathbf{Y}_s}} \tag{8}$$

where $\mathbf{C}_{\mathbf{Y}_s\mathbf{Y}_s}$ is defined as the $m \times m$ autocorrelation matrix generated between sample locations, and $\boldsymbol{\Gamma}_{\mathbf{C}_{\mathbf{Y}_s\mathbf{Y}_s}}$ is the lower triangular matrix with the dimension of $m \times m$ obtained from the Cholesky decomposition (e.g., Cherny 2005; Li et al. 2015) of $\mathbf{C}_{\mathbf{Y}_s\mathbf{Y}_s}$, using Eq. (8). $\mathbf{C}_{\mathbf{Y}_s\mathbf{Y}}$ is defined as the $m \times n$ autocorrelation matrix generated between sample locations and every location within Ω. Note that conditional mean $\boldsymbol{\mu}_{\mathbf{Y}|\mathbf{Y}_s}$ becomes spatially distributed mean, and the diagonal entries of conditional autocorrelation matrix, $\mathbf{C}_{\mathbf{YY}|\mathbf{Y}_s}$, are the conditional variances $\sigma^2_{Y|Y_s}$. At sample locations, the conditional variance $\sigma^2_{Y_s|Y_s}$ is 0, if measurement errors are negligible. In addition, each entry of $C_{YY|Y_s}$ depends on the absolute distance, $\Delta_{ij} = |z_i - z_j|$, but also the locations z_i and z_j. That is to say, conditioning a stationary random field on known measurement data leads to a nonstationary random field. Nonetheless, $C_{YY|Y_s}$ remains bounded and symmetric and as a positive definite matrix.

Once the conditional mean and covariance are calculated, we proceed to the generation of realizations of conditional random fields. These fields preserve the sample values at the sample locations and have many possible values at other locations. The mean of the possible values is the conditional mean, and their variability is described by their conditional variance. These conditional random fields can be produced using many random field generation algorithms such as the K-L expansion (e.g., Ghanem and Spanos 1991; Lu and Zhang 2007; Jiang et al. 2015) or the Cholesky decomposition (e.g., Srivastava et al. 2010; Li et al. 2015). In this study, the K-L expansion is adopted because it has been widely used in published literature (e.g., Ghanem and Spanos 1991; Cho 2014; Ali et al. 2014; Jiang et al. 2015; Huang and Griffiths 2015; Cai et al. 2017c) and because this method has desirable properties. For example, this method allows the random field discretization to be independent of the spatial discretization of the problem domain. Hence, we can adjust the solution precision according to the requirement of problems. In addition, this method has a wide range of applications including nonstationary and multidimensional problems. Detailed descriptions of K-L expansion properties can be found in Ghanem and Spanos (1991).

Specifically, a continuous form of conditional random field $Y_{|Y_s}$ can be represented as:

$$Y_{|Y_s}(\mathbf{l}) = Y_{|Y_s}(\mathbf{l};\theta) = \mu_{|Y_s}(\mathbf{l}) + \sum_{i=1}^{\infty} \xi_i(\theta)\sqrt{\eta_i} f_i(\mathbf{l}) \tag{9}$$

where $\xi_i(\theta)$ is a set of uncorrelated standard normal random variables and θ is the coordinates in the random events space; $\mathbf{l}$ is the function of the position vector defined over Ω; η_i and $f_i(\mathbf{l})$ are eigenvalues and eigenfunctions of the conditional autocorrelation function $\rho_{|Y_s}$, respectively. η_i and $f_i(\mathbf{l})$ are obtained by solving the homogeneous Fredholm integral equation of the second kind (Ghanem and Spanos 1991; Huang 2001; Jiang et al. 2015):

$$\int_\Omega \rho_{|Y_s}(\mathbf{l}_1, \mathbf{l}_2) f_i(\mathbf{l}) d\mathbf{l}_2 = \eta_i f_i(\mathbf{l}_1) \tag{10}$$

Ghanem and Spanos (1991) described a Galerkin type procedure for solving Eq. (10). This procedure transforms the eigenvalue problem in the continuous form (Eq. (10)) into the eigenvalue problem in a discretized form:

$$\mathbf{C}_{YY|Y_s}\mathbf{F} = \mathbf{F}\mathbf{\Lambda} \tag{11}$$

where $\mathbf{\Lambda}$ is a $n \times n$ diagonal matrix of eigenvalues η_i of $\mathbf{C}_{YY|Y_s}$; $\mathbf{F}$ is a $n \times n$ matrix whose columns are the corresponding eigenvectors $f_i(\mathbf{z})$ of $\mathbf{C}_{YY|Y_s}$. Note that eigenfunction $f_i(\mathbf{l})$ has been transformed to eigenvector $f_i(\mathbf{z})$ because $f_i(\mathbf{z})$ is only computed at the respective points of the spatial discretization of Ω. Ghanem and Spanos (1991) demonstrated that this approximation could yield satisfactory results by using a finite number of eigenmodes. Subsequently, the n eigenvalues and the n eigenvectors obtained from Eq. (11) are used to generate the conditioned random field, $\mathbf{Y}_{|Y_s}$:

$$\mathbf{Y}_{|Y_s} = \boldsymbol{\mu}_{Y|Y_s} + \sum_{i=1}^{n} \xi_i(\theta)\sqrt{\eta_i} f_i(\mathbf{z}) \tag{12}$$

Notice that Eq. (12) is different from Eq. (9) since the summation on the right-hand side of the equation is only up to n.

For implementation, after sorting the η_i and the corresponding $f_i(\mathbf{z})$ in descending order, the K-L expansion terms can be truncated up to the order of k. The value of k highly depends on the desired accuracy. While several methods (e.g., Huang 2001; Jiang et al. 2014; Cho 2014) have been proposed to determine the value of k, in this study, k is set to equal to n.

Thereafter, using $\mathbf{Y}_{|Y_s}$, the conditioned log-normal distributed random field $\mathbf{X}_{|X_s}$ in the physical space $\boldsymbol{x}$ is obtained via the transformation of Eq. (1) using $\mu_{\ln X}$ and $\sigma_{\ln X}$.

The aforementioned algorithm is used to generate unconditional or conditional soil cohesion and soil friction angle parameter realizations for the MCS. However, the generated soil cohesion parameter realizations are independent of the generated soil friction angle parameter realizations.

Incorporation of cross-correlation between cohesion and friction angle random fields

Generally, cross-correlations between c' and $\tan\phi'$ exist (e.g., Griffiths et al. 2011; Li et al. 2014, 2015; Jiang et al. 2015). For this reason, we implement an algorithm to incorporate cross-correlation between these two random fields derived from the algorithm described in the previous section. This algorithm is discussed as follows. Consider two cross-correlated, and log-normal distributed random fields, $\mathbf{X}_{c'}$ and $\mathbf{X}_{\tan\phi'}$ (vectors with a dimension of $n \times 1$) with measurement data $\mathbf{X}_{sc'}$ and $\mathbf{X}_{s\tan\phi'}$ at sample locations. Note that sample locations of $\mathbf{X}_{sc'}$ and $\mathbf{X}_{s\tan\phi'}$ are assumed the same, which is usually the case. A cross-correlation matrix $\mathbf{G}_{X_{c'}X_{\tan\phi'}}$ is obtained as $\mathbf{G}_{X_{c'}X_{\tan\phi'}} = \left(\rho_{i,j}\right)_{2\times 2}$, where 2×2 denotes the dimension of $\mathbf{G}_{X_{c'}X_{\tan\phi'}}$, $\rho_{i,j}$ is the cross-correlation coefficient between the ith random field and the jth random field in the physical space $\boldsymbol{x}$, where $i = \mathbf{X}_{c'}, \mathbf{X}_{\tan\phi'}$ and $j = \mathbf{X}_{c'}, \mathbf{X}_{\tan\phi'}$. Using the transformation of Eq. (1), the corresponding cross-correlated standard normal random field $\mathbf{Y}_{c'}$ and $\mathbf{Y}_{\tan\phi'}$ and the measurement data $\mathbf{Y}_{sc'}$ and $\mathbf{Y}_{s\tan\phi'}$ in the transformed standard normal space $\boldsymbol{y}$ are obtained. The cross-correlation matrix $\mathbf{G}_{Y_{c'}Y_{\tan\phi'}} = \left(\rho_{\ln i,\ln j}\right)_{2\times 2}$ is derived (Fenton and Griffiths 2008) as

$$\rho_{\ln i,\ln j} = \ln\left(1 + \rho_{i,j}\mathrm{cov}_i\mathrm{cov}_j\right) / \sqrt{\ln\left(1+\mathrm{cov}_i^2\right)\ln\left(1+\mathrm{cov}_j^2\right)} \quad \left(i = \mathbf{X}_{c'}, \mathbf{X}_{\tan\phi'}\ \ j = \mathbf{X}_{c'}, \mathbf{X}_{\tan\phi'}\right) \tag{13}$$

where $\mathrm{cov}_i = \sigma_i/\mu_i$ is the coefficient of variation of i. Subsequently, the Cholesky decomposition is used to factor $\mathbf{G}_{Y_{c'}Y_{\tan\phi'}}$, and the lower triangular matrix $\boldsymbol{\Gamma}_{G_{Y_{c'}Y_{\tan\phi'}}}$ with the dimension of 2×2 is obtained:

$$\mathbf{G}_{\mathbf{Y}_{c'}\mathbf{Y}_{\tan\phi'}} = \boldsymbol{\Gamma}_{\mathbf{G}_{\mathbf{Y}_{c'}\mathbf{Y}_{\tan\phi'}}} \boldsymbol{\Gamma}^T_{\mathbf{G}_{\mathbf{Y}_{c'}\mathbf{Y}_{\tan\phi'}}} \quad (14)$$

The transformation between the cross-correlated standard normal random fields ($\mathbf{Y}_{c'}$ and $\mathbf{Y}_{\tan\phi'}$) and the independent standard normal random fields ($\mathbf{Y}'_{c'}$ and $\mathbf{Y}'_{\tan\phi'}$) is completed using:

$$\left(\mathbf{Y}_{c'}, \mathbf{Y}_{\tan\phi'}\right) = \left(\mathbf{Y}'_{c'}, \mathbf{Y}'_{\tan\phi'}\right)\boldsymbol{\Gamma}^T_{\mathbf{G}_{\mathbf{Y}_{c'}\mathbf{Y}_{\tan\phi'}}} \quad (15)$$

First, the cross-correlated measurements $\mathbf{Y}_{sc'}$ and $\mathbf{Y}_{s\tan\phi'}$ are transformed to independent ones using Eq. (15), denoted as $\mathbf{Y}'_{sc'}$ and $\mathbf{Y}'_{s\tan\phi'}$. Next, the method described in the section "Generating conditioned random soil strength parameter field" is applied to generate two independent conditioned standard normal random fields $\mathbf{Y}'_{c'|\mathbf{Y}'_{sc'}}$ and $\mathbf{Y}'_{\tan\phi'|\mathbf{Y}'_{s\tan\phi'}}$, respectively. The cross-correlated conditioned standard normal random fields $\mathbf{Y}_{c'|\mathbf{Y}_{sc'}}$ and $\mathbf{Y}_{\tan\phi'|\mathbf{Y}_{s\tan\phi'}}$ are then generated using Eq. (15). Again, the cross-correlated conditioned log-normally distributed random fields $\mathbf{X}_{c'|\mathbf{X}_{sc'}}$ and $\mathbf{X}_{\tan\phi'|\mathbf{X}_{s\tan\phi'}}$ in the physical space $\boldsymbol{x}$ are obtained via Eq. (1).

Based on this algorithm, unconditional or conditional soil cohesion and soil friction angle parameter fields, which are correlated or mutually independent of each other, can be generated for the MCS.

Modeling of FS_i, FS, and Pf

Once unconditional or conditional random realizations of pairs of c' and $\tan\phi'$ random fields are generated, the next step is to link the random fields to a physical model that can be used to determine FS_i random field associated with each potential slip surface. The physical model is discussed below.

Without considering deformation (or neglecting stress-strain relationship), the factor of safety along the ith potential slip surface (i.e., FS_i) of an infinite slope can be evaluated using the LEM. In this study, we further assume that there is no presence of water or fluid pressure in the slope. Consequently, FS_i can be expressed as follows (e.g., Griffiths et al. 2011; Cho 2014; Li et al. 2014; Ali et al. 2014):

$$\mathrm{FS}_i = \frac{c'_i}{z_i\gamma\sin\beta\cos\beta} + \frac{\tan\phi'_i}{\tan\beta} \quad (z_i \le H) \quad (16)$$

where β is the slope inclination, γ is the total unit weight, H denotes the vertical distance of soils from the slope base to the land surface, c'_i and ϕ'_i are the effective cohesion and the effective soil friction angle at the ith potential slip surface, and z_i is the depth (positive downward) of the ith potential slip surface (see Fig. 2).

Based on Eq. (16), the random fields of c' and $\tan\phi'$ thus can be converted to FS_i random field associated with each potential slip surface over the entire slope. These FS_i random fields are used to determine the lower bounds LB_i and, in turn, the sampling location for the adaptive sampling approach as described in the "Adaptive sampling strategy" section. In addition, they can be employed to calculate the FS and Pf for the entire slope as discussed below.

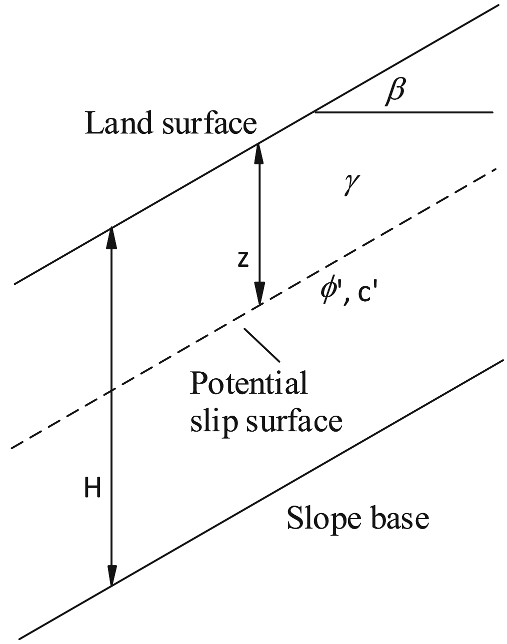

Fig. 2 An infinite slope model

FS for the entire slope is:

$$\mathrm{FS} = \min\{\mathrm{FS}_i\} = \min\left\{\frac{c'_i}{z_i\gamma\sin\beta\cos\beta} + \frac{\tan\phi'_i}{\tan\beta}\right\} \quad (z_i \le H, i = 1, \cdots, n) \quad (17)$$

The system failure probability Pf then can be evaluated using:

$$\mathrm{Pf} = \frac{1}{N_r}\sum_{i=1}^{N_r} I(\mathrm{FS} < 1) \quad (18)$$

where N_r is the number of realizations generated during MCS. $I(\cdot)$ denotes the indicator function. That is, for a realization, $I(\mathrm{FS} < 1)$ is equal to 1 when FS < 1 occurs, and 0 otherwise (e.g., Li et al. 2013; Jiang et al. 2015).

First-order estimation of $\mathrm{LB_i}$

As discussed in the "Adaptive sampling strategy" section, the adaptive sampling approach relies on the LB_i, ($\mu_{\mathrm{FS}_i} - 3\sigma_{\mathrm{FS}_i}$). The μ_{FS_i} and σ_{FS_i} to determine the LB_i can be calculated via statistical analysis of MCS realizations of FS_i evaluated at the ith potential slip surface as discussed above. However, MCS is inefficient; it requires to generate a large number of realizations to ensure that the unbiased statistics can be obtained. In order to address this issue, an efficient method called first-order analysis (e.g., Mao et al. 2011, 2013; Sun et al. 2013; Cai et al. 2016, and many others) is introduced to approximate the LB_i.

That is, using Eq. (1)–Eq. (8), one can derive the conditional mean and the conditional autocorrelation matrix of $\mathbf{Y}_{c'}$ and $\mathbf{Y}_{\tan\phi'}$, and they are $\boldsymbol{\mu}_{\mathbf{Y}_{c'}|\mathbf{Y}_{sc'}}$, $\mathbf{C}_{\mathbf{Y}_{c'}|\mathbf{Y}_{sc'}}$, and $\boldsymbol{\mu}_{\mathbf{Y}_{\tan\phi'}\big|\mathbf{Y}_{s\tan\phi'}}$, $\mathbf{C}_{\mathbf{Y}_{\tan\phi'}\big|\mathbf{Y}_{s\tan\phi'}}$, respectively. Similarly, one can compute the conditional cross-correlation matrix between $\mathbf{Y}_{c'}$ and $\mathbf{Y}_{\tan\phi'}$, denoted as $\mathbf{C}_{\mathbf{Y}_{c'\tan\phi'}\big|\mathbf{Y}_{sc's\tan\phi'}}$ using these equations. Subsequently, the conditional mean vectors, conditional autocovariance matrices, and cross-covariance matrix of $\ln c'$ and $\ln\tan\phi'$ are evaluated as follows:

$$\boldsymbol{\mu}_{\ln c'|sc'} = \sigma_{\ln X_{c'}} \boldsymbol{\mu}_{Y_{c'}|Y_{sc'}} + \mu_{\ln X_{c'}} \quad (19a)$$

$$\boldsymbol{\mu}_{\ln\tan\phi'|s\tan\phi'} = \sigma_{\ln X_{\tan\phi'}} \boldsymbol{\mu}_{Y_{\tan\phi'}|Y_{s\tan\phi'}} + \mu_{\ln X_{\tan\phi'}} \quad (19b)$$

$$\mathbf{R}_{\ln c'|sc'} = \sigma^2_{\ln X_{c'}} \mathbf{C}_{Y_{c'}|Y_{sc'}} \quad (19c)$$

$$\mathbf{R}_{\ln\tan\phi'|s\tan\phi'} = \sigma^2_{\ln X_{\tan\phi'}} \mathbf{C}_{Y_{\tan\phi'}|Y_{s\tan\phi'}} \quad (19d)$$

$$\mathbf{R}_{\ln c'\ln\tan\phi'|sc'\,s\tan\phi'} = \sigma_{\ln X_{c'}} \sigma_{\ln X_{\tan\phi'}} \mathbf{C}_{Y_{c'\tan\phi'}|Y_{sc'\,s\tan\phi'}} \quad (19e)$$

The statistical properties of $\ln FS_i$ at the ith surface are approximated using the first-order analysis based on Taylor series expansion. That is,

$$\boldsymbol{\mu}_{\ln FS} \approx \ln\left(\frac{e^{\boldsymbol{\mu}_{\ln c'|sc'}}}{z_i\gamma\sin\beta\cos\beta} + \frac{e^{\boldsymbol{\mu}_{\ln\tan\phi'|s\tan\phi'}}}{\tan\beta}\right) \quad (z_i \le H \;\; i = 1, \cdots, n) \quad (20a)$$

$$\mathbf{R}_{\ln FS \ln FS} \approx \mathbf{J}_{\ln FS \ln c'} \mathbf{R}_{\ln c'|sc'} \mathbf{J}^T_{\ln FS \ln c'} + \mathbf{J}_{\ln FS \ln\tan\phi'} \mathbf{R}_{\ln\tan\phi'|s\tan\phi'} \mathbf{J}^T_{\ln FS \ln\tan\phi'} + \mathbf{J}_{\ln FS \ln c'} \mathbf{R}_{\ln c'\ln\tan\phi'|sc'\,s\tan\phi'} \mathbf{J}^T_{\ln FS \ln\tan\phi'} + \mathbf{J}_{\ln FS \ln\tan\phi'} \mathbf{R}^T_{\ln c'\ln\tan\phi'|sc'\,s\tan\phi'} \mathbf{J}^T_{\ln FS \ln c'} \quad (20b)$$

where $\mathbf{J}_{\ln FS \ln\tan\phi'}$, $\mathbf{J}_{\ln FS \ln c'}$ are $n \times n$ diagonal sensitivity matrices of $\ln FS_i$ ($i = 1, \cdots, n$) with respect to changes in $\ln\tan\phi'_i$ and $\ln c'_i$ of different z_i ($i = 1, \cdots, n$), respectively. Each diagonal entry of $\mathbf{J}_{\ln FS \ln\tan\phi'}$ and $\mathbf{J}_{\ln FS \ln c'}$ is calculated by:

$$J_{\ln FS_i \ln\tan\phi'_i} = \left.\frac{\partial \ln FS_i}{\partial \ln\tan\phi'_i}\right|_{\left(\mu_{i,\ln c'|sc'},\, \mu_{i,\ln\tan\phi'|s\tan\phi'}\right)} = \frac{1}{1 + e^{\left(\mu_{i,\ln c'|sc'} - \mu_{i,\ln\tan\phi'|s\tan\phi'}\right)} / (z_i\gamma\cos^2\beta)} \quad (21a)$$

$$J_{\ln FS_i \ln c'_i} = \left.\frac{\partial \ln FS_i}{\partial \ln c'_i}\right|_{\left(\mu_{i,\ln c'|sc'},\, \mu_{i,\ln\tan\phi'|s\tan\phi'}\right)} = \frac{1}{z_i\gamma\cos^2\beta\, e^{\left(\mu_{i,\ln\tan\phi'|s\tan\phi'} - \mu_{i,\ln c'|sc'}\right)} + 1} \quad (21b)$$

where $i = 1, \cdots, n$; $\boldsymbol{\mu}_{\ln FS}$ is the $n \times 1$ conditional mean vector for $\ln FS_i$ ($i = 1, \cdots, n$); $\mathbf{R}_{\ln FS \ln FS}$ is the $n \times n$ conditional auto-covariance matrix for $\ln FS_i$ ($i = 1, \cdots, n$).

The diagonal entries of $\mathbf{R}_{\ln FS \ln FS}$ are the conditional variance $\boldsymbol{\sigma}^2_{\ln FS}$ for $\ln FS_i$ ($i = 1, \cdots, n$). The LB_i is then determined by $\mu_{\ln FS_i} - 3\sigma_{\ln FS_i}$ in logarithm form. This first-order approach thus avoids the brute-force MCS approach for selecting sampling locations.

Illustrative example

The usefulness of the proposed adaptive sampling approach is demonstrated using borehole data from Central Business District, Perth, Western Australia (Li et al. 2016a). The profiles of soil strength parameters, c' and $\tan\phi'$, along six boreholes (BH1 through BH6) are displayed in Fig. 3a and b, respectively. As shown in the figures, three types of soil layers (i.e., clay, sand, and silt) present over the depth of 28 m. The thickness of soil layers ranges from 0.3 to 8.7 m. Soil strength data from the six boreholes are first used to estimate the prior statistics of the soil strength parameter to obtain the unconditional stochastic description of the spatial variability of the soil parameters for the entire field site.

The unconditional statistics of c' and $\tan\phi'$ based on the six borehole data are tabulated in Table 1, including a mean and standard deviation of c' denoted as $\mu_{c'}$ and $\sigma_{c'}$, mean and standard deviation of $\tan\phi'$ denoted as $\mu_{\tan\phi'}$ and $\sigma_{\tan\phi'}$, cross-correlation coefficient $\rho_{c'\tan\phi'}$ and correlation scale λ,along the borehole direction (i.e., z-direction). Variogram analysis indicates that λ is about 6.4 m, which is about the average thickness of all layers. This result substantiates the physical meaning of λ, which is the average dimension (e.g., length, thickness) of heterogeneity (e.g., layers, or stratifications) at a field site (Yeh et al. 2015a).

Subsequently, these prior statistics and different sampling approaches are applied to determine the slope stability of a reference slope, which is assumed to be consisting of perfectly stratified layers so as the LEM physical model is applicable. Table 1 also lists the slope geometry parameters (i.e., slope high, angle, and unit weight).

FS_i profile of the reference c' - $\tan\phi'$ slope

This reference slope is discretized into 280 potential slip surfaces first. Then, c' and $\tan\phi'$ profiles of BH4 are mapped to the potential slip surfaces as the "real" distributions of c' and $\tan\phi'$ of this reference slope. The "correct" FS_i for each potential slip surface of the reference slope is illustrated in Fig. 4. The FS calculated using these "real" profiles is 1.0961 with the critical slip surface at depth 24.45 m. They are viewed as the "correct" FS and "correct" slip surface, respectively. Because the "correct" FS is greater than 1, the reference slope is considered stable, and the "correct" Pf is 0.

Effect of random sampling on estimation of FS and reliability of slope

In order to demonstrate the effectiveness of the adaptive sampling approach, we first investigate the case where a sample (measurement) is taken at random from the 280 potential slip surfaces for conditioning until all the 280 potential slip surfaces are considered. For each sample, 100,000 realizations are employed to conduct the conditional MCS. Figure 5a–d displays the sample locations and conditional Pf and FS statistics (μ_{FS} and σ_{FS}), respectively, associated with 0, 10, 20, …, 280 sample(s) (indicated along the horizontal axes).

As illustrated in Fig. 5b, with the increase in the number of samples, the Pf approaches the "correct" Pf, which is 0. That is, the mean of FS, μ_{FS}, becomes the "correct" FS (Fig. 5c), which is greater than 1 (the slope is stable), and σ_{FS}, representing the uncertainty of FS, gradually reduces to 0 (Fig. 5d).

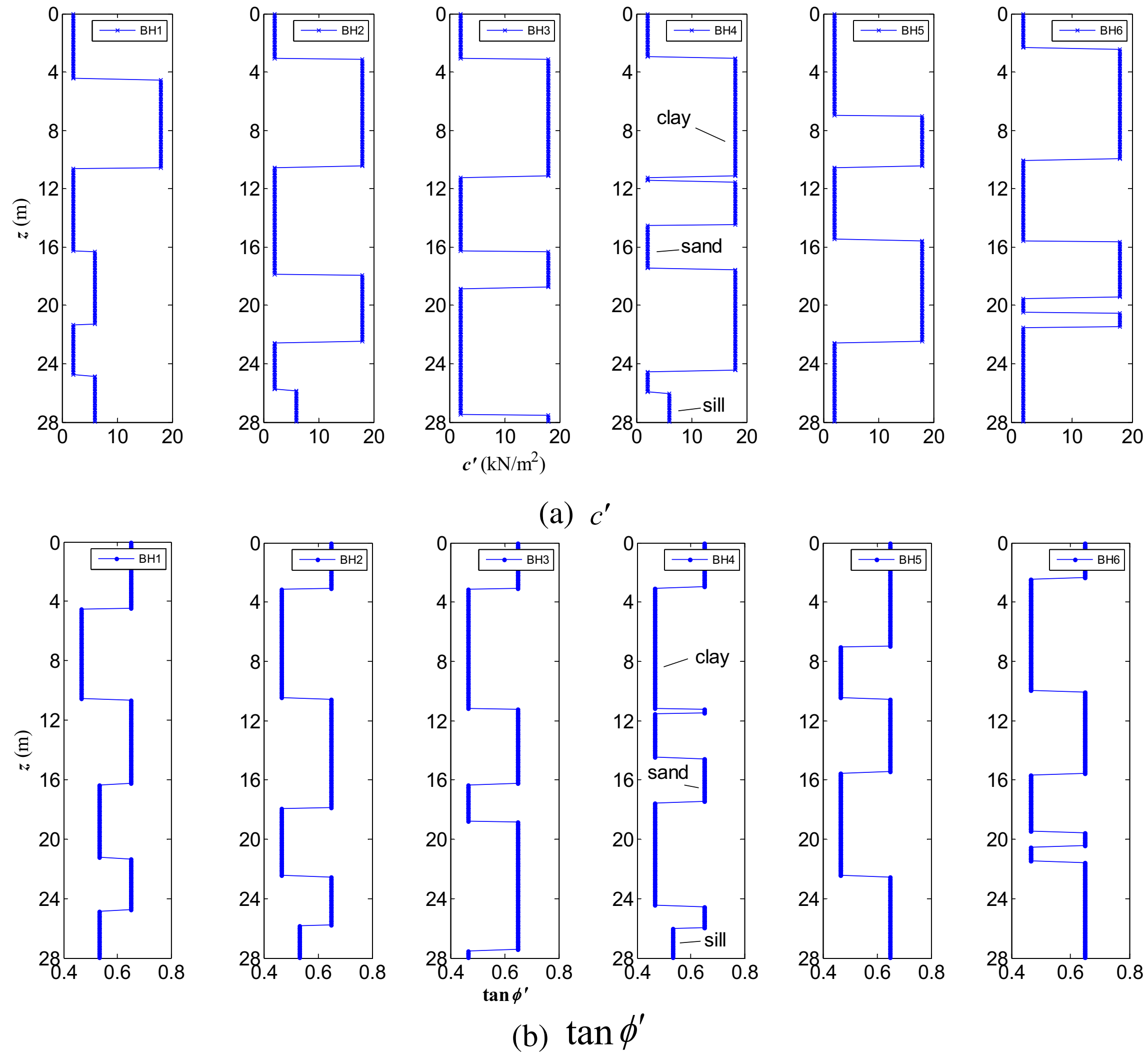

Fig. 3 **a**, **b** Profiles of soil strength parameters (BH1–BH6) in Perth City, Australia (according to Li et al. 2016a)

Table 1 Prior statistics of c' and $\tan\phi'$ based on borehole data and slope geometry parameters

Parameters	Values
Mean of c', $\mu_{c'}$	9.0 kN/m^2
Standard deviation of c', $\sigma_{c'}$	7.71 kN/m^2
Mean of $\tan\phi'$, $\mu_{\tan\phi'}$	0.564
Standard deviation of $\tan\phi'$, $\sigma_{\tan\phi'}$	0.0882
Cross-correlation coefficient between c' and $\tan\phi'$, $\rho_{c'\tan\phi'}$	− 0.664
Correlation scale in borehole direction based on variogram analysis, λ	6.4 m
Slope height, H	28 m
Slope angle, β	25°
Total unit weight, γ	20 kN/m^3

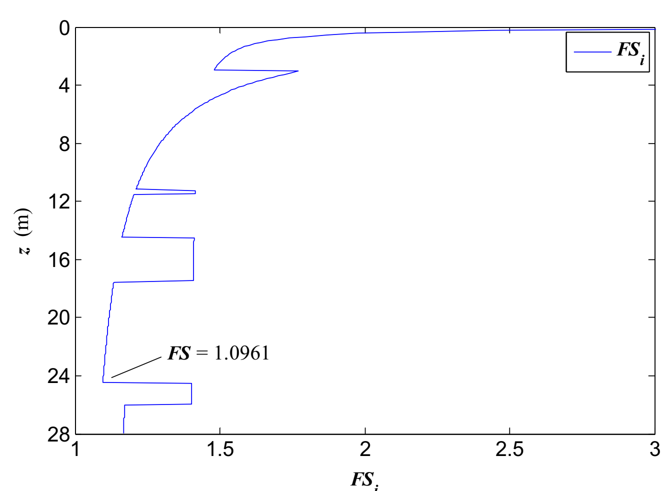

Fig. 4 The "correct" FS_i profile of the reference slope

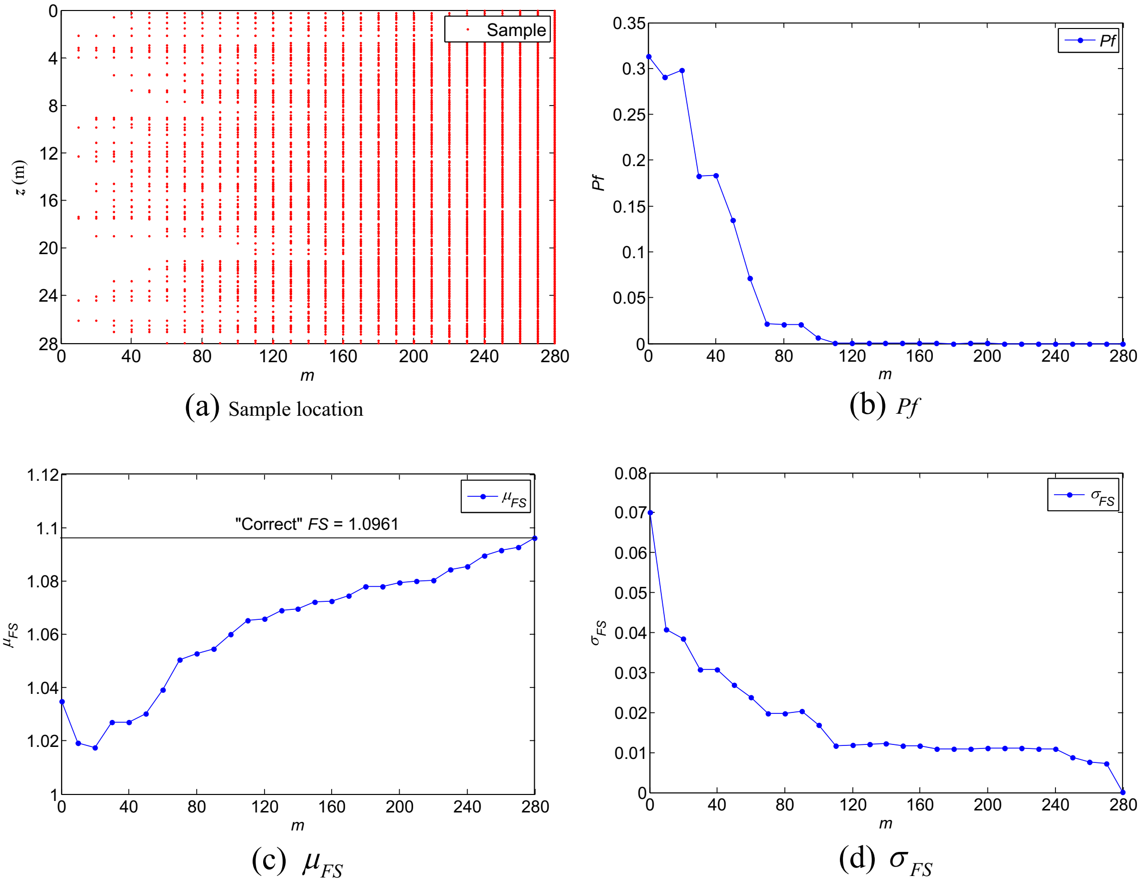

Fig. 5 **a**–**d** Sample locations and Pf and FS statistics associated with increasing number of samples (m is sample number) by random sampling based on MCS with 100,000 realizations

Notice that in Fig. 5b, Pf is reduced close to 0 after 110 samples are included, and the value of σ_{FS} remains around 0.012 even after the inclusion of 110 samples. It finally becomes 0 once all the 280 samples are used for conditioning, meanwhile μ_{FS} approaches "correct" FS. These results indicate that μ_{FS} and σ_{FS} do not behave the same way as does Pf, since μ_{FS} and σ_{FS} vary with the conditional distribution of FS, while Pf represents the percentage of FSs that is smaller than 1 (the limit equilibrium state). These results reveal the difficulty of estimating the exact FS, and the necessity of a stochastic analysis to derive the uncertainty of the FS estimate.

The LB$_i$ (i.e., $\mu_{\mathrm{FS}_i}-3\sigma_{\mathrm{FS}_i}$) along the slope based on 100,000 FS$_i$ realizations conditioned with 30 samples is shown as a solid black

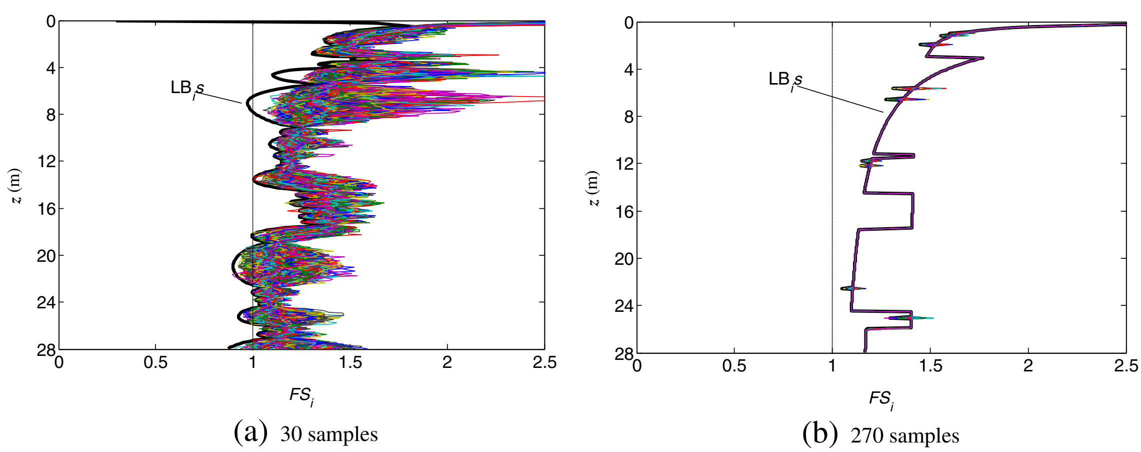

Fig. 6 **a**, **b** LB$_i$s (generated based on 100,000 realizations) and 1000 realizations of FS$_i$ ($i = 1, \cdots, n$) (among 100,000 realizations) conditioning with 30 and 270 samples, respectively

line in Fig. 6a. Color lines in the figure represent selected 1000 FS_i profiles from the 100,000 realizations, and the vertical long-dashed line represents the limit equilibrium state (i.e., FS = 1). The LB_is based on 100,000 FS_i realizations, and the 1000 realizations conditioned with 270 samples are illustrated as a solid black line and color lines in Fig. 6b, respectively. Because of a large number of conditioning data, the two lines are distinguishable only at the 10 unconditioned locations. As demonstrated in Fig. 6a, b, the calculated LB_i agrees with the lower bound of all possible FS_is at the ith slip surfaces. As expected, the LB_is and all FS_i profiles change as the number of samples increases and gradually converge to the "correct" FS_i field (see Fig. 4). In addition, even though after conditioning with 270 samples, there still exists uncertainty at locations where no sample is taken, leading to the uncertainty associated with the FS estimate. Meanwhile, the Pf is extremely close to 0 as the minimum value of LB_is is larger than 1 (the limit equilibrium state).

Adaptive sampling approach based on MCS

The sample locations, conditional Pf, conditional μ_{FS}, and its σ_{FS} from the adaptive sampling approach based on MCS are shown in Fig. 7a–d, respectively, with increasing number of samples; 100,000 realizations are used at each conditional MCS. Criterion 2 (i.e., Pf approaches 0) is selected for stopping this process. Comparing these results with those from the random sampling approach (Fig. 5), we observe that fewer samples are needed to obtain accurate evaluations of FS and Pf with small uncertainty. That is, only 25 samples are needed to meet criterion 2 and to obtain the conditioned Pf = 0.00169, μ_{FS} = 1.0525, σ_{FS} = 0.0142. On the other hand, the random sampling requires at least 110 samples to yield similar results.

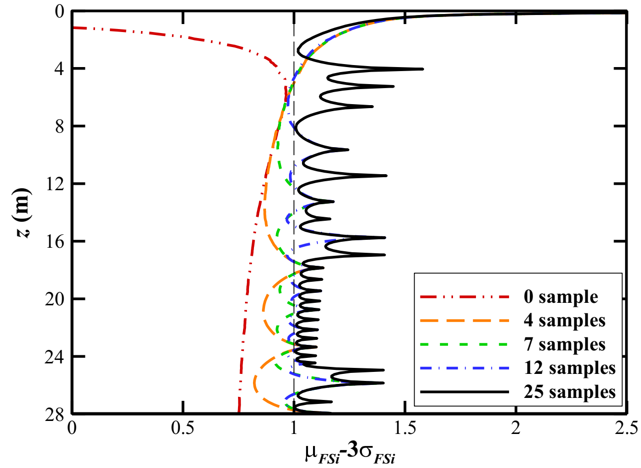

Fig. 8 Illustration of changes of LB_is using adaptive sampling approach based on MCS (each LB_is is generated based on 100,000 realizations)

Since the adaptive sampling approach is driven by the conditional LB_is, the behaviors of LB_is during the adaptive sampling process are illustrated in Fig. 8 to show the role of the sampling approach on reducing the uncertainty. These LB_is are generated based on 100,000 realizations using MCS for each new sample. Figure 8 shows that the 25 samples based on the LB_is are not equally distributed along the vertical direction of the slope.

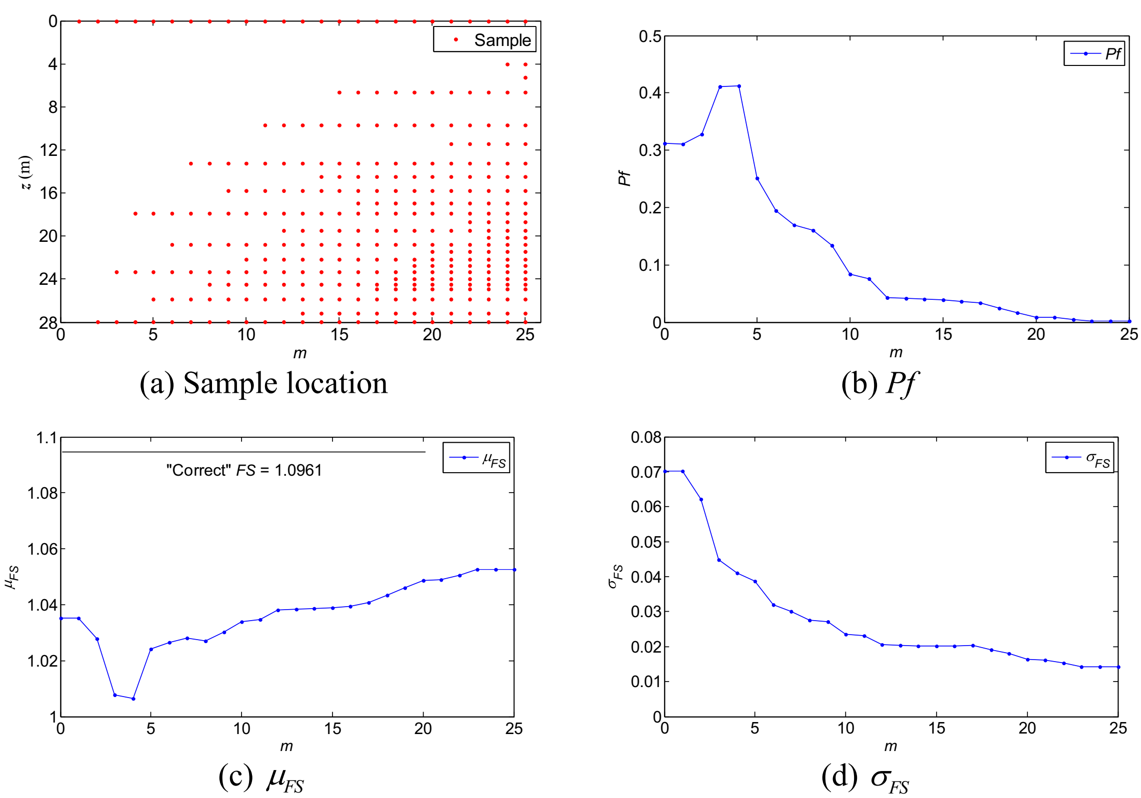

Fig. 7 **a–d** Sample locations and Pf and FS statistics associated with increasing number of samples (m is sample number) by adaptive sampling approach based on MCS with 100,000 realizations

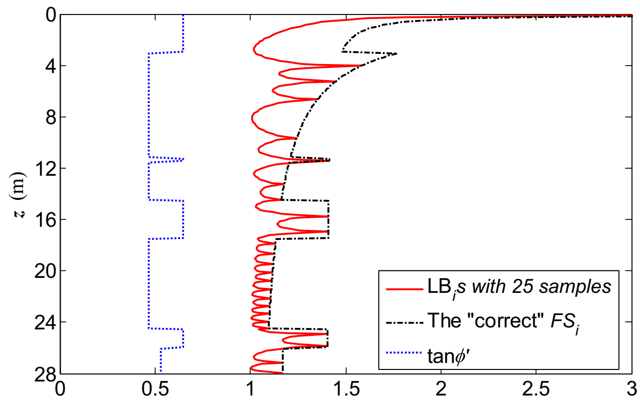

Fig. 9 Comparisons between the LB$_i$s conditioned on 25 samples using adaptive sampling approach, the "correct" FS$_i$ field and the reference profile of tanϕ'

Specifically, at the beginning, samples are taken at the interval of one correlation scale (e.g., when using 4 samples in Fig. 8), gradually, the intervals are bisected, and the samples are taken more locally. The sampling density is the largest from 18 to 25 m (i.e., the critical part) and the smallest from 0 to 12 m within the slope. This reflects the fact that in less critical areas, less samples are needed.

For better comparisons, the shape of the LB$_i$s based on 25 samples, the "correct" FS$_i$ field (see Fig. 4), and the reference profiles of soil strength parameters (i.e., tanϕ' of BH4 in Fig. 3) are redrawn in Fig. 9. As shown in Fig. 9, it is apparent that the shape of the LB$_i$s reflects the lithological heterogeneity or stratigraphy, and the likely regions of critical slip surfaces are identified. This result indicates that the effects of heterogeneity on slope stability analysis can be sufficiently characterized by a small number of samples via the adaptive sampling approach. It is, hence, not surprising to see that FS and Pf, based on this characterized result that captures the critical part of the slope, become more accurate and approach the "correct" FS and Pf (Fig. 7) as more samples are included.

Adaptive sampling approach based on first-order analysis

Although the above adaptive sampling approach is appealing, two concerns need to be addressed. First, the constant updating LB$_i$s using MCS is time-consuming. To ease this effort, the conditional first-order estimation of LB$_i$s is used (see "First-order estimation of LB$_i$" section). Second, only one sample is taken at each time and the LB$_i$s have to be updated accordingly. This step-by-step approach is inefficient since it leads to many simulations. This concern leads to a manual decision for the number of samples to be taken at each time.

This manual decision approach is demonstrated in Fig. 10a, where five samples are first taken at the interval of one correlation scale to cover the entire slope. After these five samples, we examine the shape of the LB$_i$s ($\mu_{\ln FS_i} - 3\sigma_{\ln FS_i}$) and decide the number of samples to be taken. For example, the part marked with a rectangle is more critical to FS and Pf where the values of LB$_i$s in the rectangle are smaller than the limit equilibrium state (i.e., lnFS =

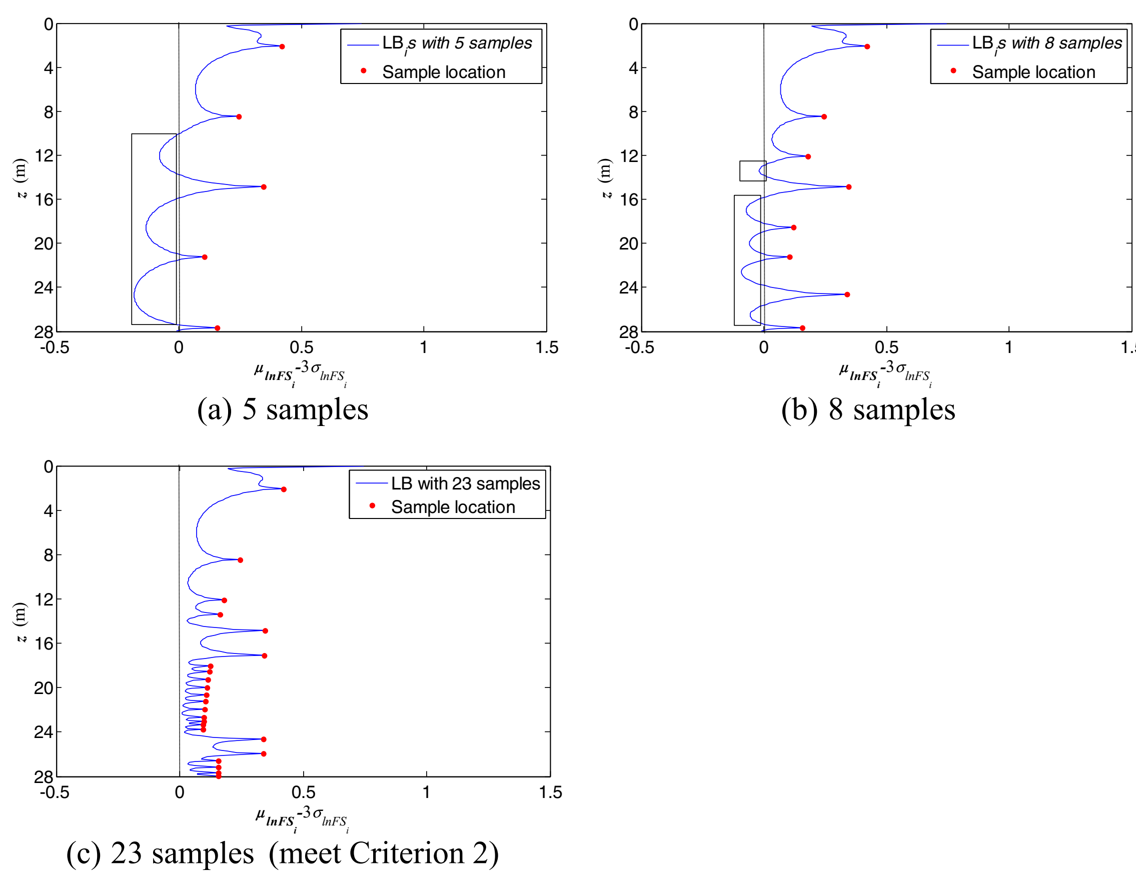

Fig. 10 a–c The adaptive sampling process with manual decision based on conditional first-order analysis

0) and values of LB_is at other parts of the slope. We therefore expect that the three "crests" vertexes in the rectangle will sequentially become the minimum point of the LB_is as the sampling process continues. Accordingly, three samples are taken at the three vertexes simultaneously. Similarly, five samples can be taken at the five vertexes marked with two rectangles in Fig. 10b afterward. Finally, 23 samples are included (Fig. 10c) in accordance with criterion 2. With these samples, we obtain conditioned Pf = 0.0012, conditional $\mu_{FS} = 1.058$, $\sigma_{FS} = 0.0140$. Apparently, this manual decision approach is more efficient than the "step-by-step" sampling approach, and it yields comparable results.

The above adaptive sampling approach implicitly suggests that the minimum number of samples required to reduce uncertainty in the stability analysis would be the ratio of the slope height to the correlation scale length of the soil strength parameter (H/λ). That is, at least one sample should be taken within each layer or stratum if the strata are known since the correlation scale represents the average thickness of the strata of the slope. Afterward, additional samples (if any) should be taken within the identified critical part of slope to reach a sufficient characterization of heterogeneity in this region. At last, the conditional MCS should be carried out to assess FS, Pf, and uncertainty.

Lastly, we must emphasize our prior knowledge of the spatial statistics of a field site is one of the keys to our adaptive sampling approach. The spatial statistics can be estimated from the available borehole data, as we demonstrated in this example.

Conclusions

It is a fact that the uncertainty of analysis of slope stability can be reduced as long as the heterogeneity of a slope is adequately characterized. Our proposed adaptive sampling approach, nevertheless, takes advantage of the conditional stochastic methodology with our prior knowledge of the spatial variability of soil strength parameters, the soil strength parameters of soil samples, and a physical model to guide our sampling efforts. In this paper, we demonstrate that using this sampling approach, we can sufficiently characterize the effects of heterogeneity on slope stability analysis using a small number of samples. Further, we can identify probable critical sections of slope, which deserves engineering control measures. Thus, the cost for preventing the failure of a slope can be greatly reduced.

Funding information

This work was supported by the Fundamental Research Funds for the Central Universities, China University of Geosciences (Wuhan) (Grant No. CUG170686); the China Scholarship Council (Grant No. 201406410032); the National Natural Science Foundation of China (Grant No. 41172282 and Grant No. 41672313); and the National Science Foundation-Division of Earth Sciences (Grant No. 1014594). The second author also acknowledges the Outstanding Oversea Professorship award through Jilin University from the Department of Education, China, as well as the Global Expert award through Tianjin Normal University from the Thousand Talents Plan of Tianjin City.

References

Ali A, Huang J, Lyamin AV, Sloan SW, Griffiths DV, Cassidy MJ, Li JH (2014) Simplified quantitative risk assessment of rainfall-induced landslides modelled by infinite slopes. Eng Geol 179:102–116. https://doi.org/10.1016/j.enggeo.2014.06.024

Brejda JJ, Moorman TB, Smith JL, Karlen DL, Allan DL, Dao TH (2000) Distribution and variability of surface soil properties at a regional scale. Soil Sci Soc Am J 64(3):974. https://doi.org/10.2136/sssaj2000.643974x

Cai J-S, Yan E, Yeh TJ, Zha Y (2016) Effects of heterogeneity distribution on hillslope stability during rainfalls. Water Sci Eng 9(2):134–144. https://doi.org/10.1016/j.wse.2016.06.004

Cai J-S, Yan E-C, Yeh T-CJ, Zha YY, Liang Y, Huang SY, Wang WK, Wen JC (2017a) Effect of spatial variability of shear strength on reliability of infinite slopes using analytical approach. Comput Geotech 81:77–86. https://doi.org/10.1016/j.compgeo.2016.07.012

Cai J-S, Yan E-C, Yeh TJ, Zha Y-Y (2017b) Sampling schemes for hillslope hydrologic processes and stability analysis based on cross-correlation analysis. Hydrol Process 31(6):1301–1313. https://doi.org/10.1002/hyp.11101

Cai J-S, Yeh TJ, Yan E-C et al (2017c) Uncertainty of rainfall-induced landslides considering spatial variability of parameters. Comput Geotech 87:149–162. https://doi.org/10.1016/j.compgeo.2017.02.009

Cherny SS (2005) Cholesky Decomposition. In B. S. Everitt & D. C. Howell (eds) Encyclopedia ofStatistics in Behavioral Science, vol 1. John Wiley & Sons, Chichester, pp 262–263. https://doi.org/10.1002/0470013192.bsa090

Cho SE (2007) Effects of spatial variability of soil properties on slope stability. Eng Geol 92(3-4):97–109. https://doi.org/10.1016/j.enggeo.2007.03.006

Cho SE (2014) Probabilistic stability analysis of rainfall-induced landslides considering spatial variability of permeability. Eng Geol 171:11–20. https://doi.org/10.1016/j.enggeo.2013.12.015

Christian J, Ladd C, Baecher G (1994) Reliability and probability in stability analysis. J Geotech Eng 120(12):2180–2207. https://doi.org/10.1061/(ASCE)0733-9410(1994)120:12(2180)

El-Ramly H, Morgenstern NR, Cruden DM (2002) Probabilistic slope stability analysis for practice. Can Geotech J 39(3):665–683. https://doi.org/10.1139/t02-034

Fenton GA, Griffiths DV (2008) Risk assessment in geotechnical engineering. Wiley, New York. https://doi.org/10.1002/9780470284704

Ghanem RG, Spanos PD (1991) Stochastic finite elements: a spectral approach. Springer, New York. https://doi.org/10.1007/978-1-4612-3094-6

Griffiths DV, Fenton GA (2004) Probabilistic slope stability analysis by finite elements. J Geotech Geoenviron Eng 130(5):507–518. https://doi.org/10.1061/(ASCE)1090-0241(2004)130:5(507)

Griffiths DV, Huang J, Fenton G a. (2011) Probabilistic infinite slope analysis. Comput Geotech 38(4):577–584. https://doi.org/10.1016/j.compgeo.2011.03.006

Harter T, Yeh TJ (1996) Conditional stochastic analysis of solute transport in heterogeneous, variably saturated soils. Water Resour Res 32(6):1597–1609. https://doi.org/10.1029/96WR00503

Huang SP (2001) Simulation of random processes using Karhunen-Loeve expansion. National University of Singapore, Singapore

Huang J, Griffiths DV (2015) Determining an appropriate finite element size for modelling the strength of undrained random soils. Comput Geotech 69:506–513. https://doi.org/10.1016/j.compgeo.2015.06.020

Jiang S-H, Li D-Q, Zhang L-M, Zhou C-B (2014) Slope reliability analysis considering spatially variable shear strength parameters using a non-intrusive stochastic finite element method. Eng Geol 168:120–128. https://doi.org/10.1016/j.enggeo.2013.11.006

Jiang S-H, Li D-Q, Cao Z-J, Zhou CB, Phoon KK (2015) Efficient system reliability analysis of slope stability in spatially variable soils using Monte Carlo simulation. J Geotech Geoenviron Eng 141(2):4014096. https://doi.org/10.1061/(ASCE)GT.1943-5606.0001227

Li L, Wang Y, Cao Z, Chu X (2013) Risk de-aggregation and system reliability analysis of slope stability using representative slip surfaces. Comput Geotech 53:95–105. https://doi.org/10.1016/j.compgeo.2013.05.004

Li D-Q, Qi X-H, Phoon K-K, Zhang LM, Zhou CB (2014) Effect of spatially variable shear strength parameters with linearly increasing mean trend on reliability of infinite slopes. Struct Saf 49:45–55. https://doi.org/10.1016/j.strusafe.2013.08.005

Li D-Q, Jiang S-H, Cao Z-J, Zhou W, Zhou CB, Zhang LM (2015) A multiple response-surface method for slope reliability analysis considering spatial variability of soil properties. Eng Geol 187:60–72. https://doi.org/10.1016/j.enggeo.2014.12.003

Li D-Q, Qi X-H, Cao Z-J, Tang XS, Phoon KK, Zhou CB (2016a) Evaluating slope stability uncertainty using coupled Markov chain. Comput Geotech 73:72–82. https://doi.org/10.1016/j.compgeo.2015.11.021

Li XY, Zhang LM, Li JH (2016b) Using conditioned random field to characterize the variability of geologic profiles. J Geotech Geoenviron Eng 142(4):4015096. https://doi.org/10.1061/(ASCE)GT.1943-5606.0001428

Lloret-Cabot M, Fenton GA, Hicks MA (2014) On the estimation of scale of fluctuation in geostatistics. Georisk Assess Manag Risk Eng Syst Geohazards 8(2):129–140. https://doi.org/10.1080/17499518.2013.871189

Lu Z, Zhang D (2007) Stochastic simulations for flow in nonstationary randomly heterogeneous porous media using a KL-based moment-equation approach. Multiscale Model Simul 6(1):228–245. https://doi.org/10.1137/060665282

Mao D, Wan L, Yeh TJ et al (2011) A revisit of drawdown behavior during pumping in unconfined aquifers. Water Resour Res 47(5):W05502. https://doi.org/10.1029/2010WR009326

Mao D, Yeh T-CJ, Wan L, Lee CH, Hsu KC, Wen JC, Lu W (2013) Cross-correlation analysis and information content of observed heads during pumping in unconfined aquifers. Water Resour Res 49(2):713–731. https://doi.org/10.1002/wrcr.20066

Parkin TB, Robinson JA (1992) Analysis of Lognormal Data. In: Stewart B.A. (eds) Advances in Soil Science. Advances in Soil Science, vol 20. Springer, New York, pp 193–235. https://doi.org/10.1007/978-1-4612-2930-8_4

Parkin TB, Meisinger JJ, Starr JL, Chester ST, Robinson JA (1988) Evaluation of statistical estimation methods for lognormally distributed variables. Soil Sci Soc Am J 52(2):323. https://doi.org/10.2136/sssaj1988.03615995005200020004x

Phoon K-K, Kulhawy FH (1999) Characterization of geotechnical variability. Can Geotech J 36(4):612–624. https://doi.org/10.1139/t99-038

Srivastava A, Babu GLLS, Haldar S (2010) Influence of spatial variability of permeability property on steady state seepage flow and slope stability analysis. Eng Geol 110(3-4):93–101. https://doi.org/10.1016/j.enggeo.2009.11.006

Sun R, Yeh TJ, Mao D et al (2013) A temporal sampling strategy for hydraulic tomography analysis. Water Resour Res 49(7):3881–3896. https://doi.org/10.1002/wrcr.20337

van den Eijnden AP, Hicks MA (2011) Conditional simulation for characterising the spatial variability of sand state. In: Proc. 2nd Int. Symp. Comp. Geomech. Croatia, pp 288–296

Vanmarcke EH (1977a) Probabilistic modeling of soil profiles. J Geotech Eng Div 103:1227–1246

Vanmarcke EH (1977b) Reliability of earth slopes. J Geotech Eng Div 103:1247–1265

Wang Y, Cao Z, Li D (2016) Bayesian perspective on geotechnical variability and site characterization. Eng Geol 203:117–125. https://doi.org/10.1016/j.enggeo.2015.08.017

Yeh T-C, Khaleel R, Carroll KC (2015a) Flow through heterogeneous geologic media. Cambridge University Press, New York. https://doi.org/10.1017/CBO9781139879323

Yeh T-C, Mao D, Zha Y et al (2015b) Uniqueness, scale, and resolution issues in groundwater model parameter identification. Water Sci Eng 8(3):175–194. https://doi.org/10.1016/j.wse.2015.08.002

Zhang J, Zhang LM, Tang WH (2011) New methods for system reliability analysis of soil slopes. Can Geotech J 48(7):1138–1148. https://doi.org/10.1139/t11-009

J.-S. Cai · E.-C. Yan · R.-X. Tang
Faculty of Engineering,
China University of Geosciences,
Wuhan, 430074, China

T.-C. J. Yeh
Key Laboratory for Water Environment and Resources,
Tianjin Normal University,
Tianjin, China

T.-C. J. Yeh (✉)
Department of Hydrology & Atmospheric Sciences,
The University of Arizona,
1133 E. James E. Rogers Way, 122 Harshbarger Bldg 11, Tucson, AZ 85721, USA
Email: yeh@hwr.arizona.edu

J.-C. Wen
Department of Safety, Health and Environmental Engineering,
National Yunlin University of Science and Technology,
Douliu, Taiwan

J.-C. Wen
Research Center for Soil and Water Resources and Natural Disaster Prevention,
National Yunlin University of Science and Technology,
Douliu, Taiwan

S.-Y. Huang
Graduate School of Engineering Science and Technology,
National Yunlin University of Science and Technology,
Douliou, Taiwan